8 Surface Characterization

Mandla A. Tshabalala

USDA, Forest Service, Forest Products Laboratory, Madison, WI

CONTENTS

8.1 OVERVIEW OF SURFACE PROPERTIES

Surface properties of wood play an important role when wood is used or processed into different commodities such as siding, joinery, textiles, paper, sorption media or wood composites. Thus, for example, the quality and durability of a wood coating are determined by the surface properties of the wood and the coating. The same is true for wood composites, as the efficiency of stress transfer from the wood component to the non-wood component is strongly influenced by the surface properties of both components.

Surface properties of wood can be divided into two major groups: physical and chemical properties. Physical properties include morphology, roughness, smoothness, specific surface area and permeability. Chemical properties include elemental and molecular, or functional, group composition. Together, these two major groups of properties determine the thermodynamic characteristics of the wood surface, such as surface free energy and surface acid-base acceptor and donor numbers.

Wood has a cellular structure, the cell walls of which are composed of three major constituents: cellulose, hemicelluloses, and lignin. In addition to these major constituents, the cell walls also contain pectins, extractives and trace metals. The surface properties of wood are therefore determined by the morphology of the cell wall at the surface of a wood element (particle, fiber, flake, or chip), and the distribution of the major and minor constituents in the cell wall. Hence, to optimize the interaction between a wood surface and a coating, or a matrix in a wood composite,

the surface properties of both the wood and the coating, or the matrix in a composite, must be known.

Methods for characterizing surface properties of wood may be divided into three broad categories: microscopic, spectroscopic, and thermodynamic. Microscopic methods provide information about surface morphology; spectroscopic methods provide information about surface chemistry, and thermodynamic methods provide information about the surface energy.

8.2 MICROSCOPIC METHODS FOR CHARACTERIZING SURFACE PROPERTIES

Many types of microscopic methods are available for characterizing the physical properties of various material surfaces, but only a few have been particularly useful for characterizing the physical properties of wood surfaces: Confocal laser scanning microscopy (CLSM), scanning electron microscopy (SEM), and atomic force microscopy (AFM).

8.2.1 CONFOCAL LASER SCANNING MICROSCOPY

A typical confocal laser scanning microscopy (CLSM) instrument consists of a light microscope equipped with scanning mechanisms and a motorized focus, a laser source (He/Ne, krypton or argon), and a computer system with software for instrument control, three-dimensional (3-D) reconstruction, and image processing and analysis.

The basic principle of CLSM is illustrated schematically in Figure 8.1. A collimated, polarized laser beam from an aperture is reflected by a beam splitter (dichroic mirror) into the rear of the objective lens and is focused on the specimen. The reflected, or emitted, longer-wavelength fluorescent light returning from the specimen passes back through the same lens. The light beam is focused by the beam splitter into a small pinhole, the confocal aperture, to eliminate all of the out-of-focus light that comes from regions of the specimen that are above or below the plane of focus. A photo multiplier tube (PMT), positioned behind the confocal aperture, converts the detected in-focus light beam from each specimen point into an analog output signal, which is stored in a computer in digital form. A point-by-point digital image is obtained by scanning the beam over an XY plane. The thickness of such an XY image in the Z direction depends on the diameter of the detector pinhole: the more open the pinhole, the thicker the XY image (Pawley 1990, Boyde 1994, Lichtman 1994, Béland and Mangin 1995, Leica 1999).
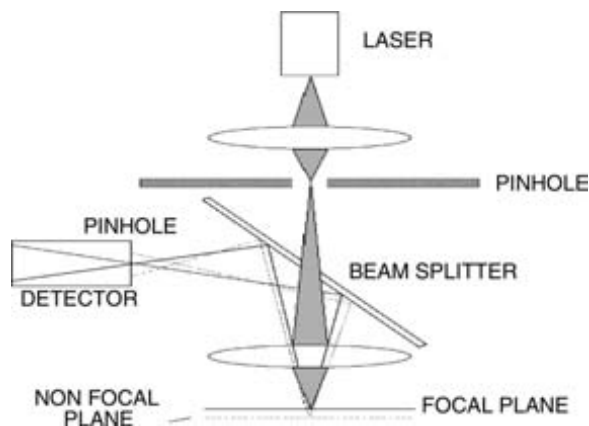

FIGURE 8.1 Principle of CLSM. Out-of-focus light beam from non focal plane is excluded from the detector by the confocal detector pinhole. (Courtesy of Lloyd Donaldson, M.Sc. Hons, D. Sc. Cell Wall Biotechnology Center, Forest Research, New Zealand.)
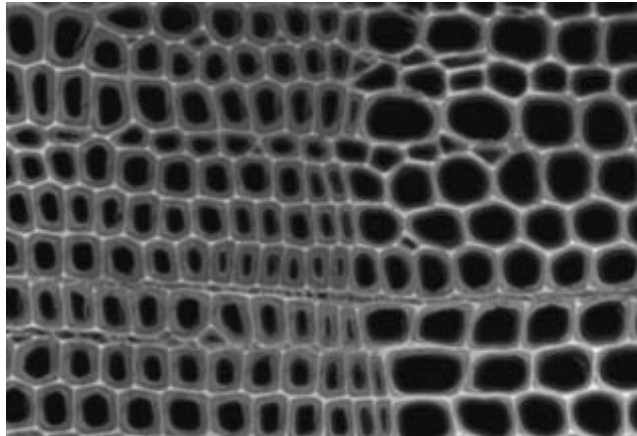
FIGURE 8.2 Transverse view of thick-wall latewood (left) and thin-wall early wood (right) tracheids of *Pinus radiata.*(Micrographs provided by Lloyd Donaldson, M.Sc. Hons, D.Sc. Cell Wall Biotechnology Center, Forest Research, New Zealand.)

Perhaps the greatest advantage of CLSM over other forms of optical microscopy is that it allows 3-D imaging of thick and opaque specimens, such as wood surfaces, without physically slicing the specimen into sections. Figures 8.2–8.4 show 625- $\times$ 625-µm micrographs of a wood specimen that were obtained with a Leica TCS/NT confocal microscope. The wood specimen was stained with acriflavin (Donaldson 2003). The micrographs clearly show the anisotropic morphology of wood surfaces. In the transverse view (Figure 8.2) thin-walled earlywood and thick-walled latewood tracheids are clearly distinguishable. In the radial view (Figure 8.3) radial bordered pits and a uniseriate heterogeneous ray are clearly visible. In the tangential view (Figure 8.4) uniseriate rays, small tangential pits in latewood, and larger tangential pits in earlywood are also clearly visible.

CLSM has also been used in the study of resin distribution in medium density fiberboard (Loxton et al. 2003). In another study, CLSM was used to study the effect of simulated acid rain on coatings for exterior wood panels (Lee et al 2003).
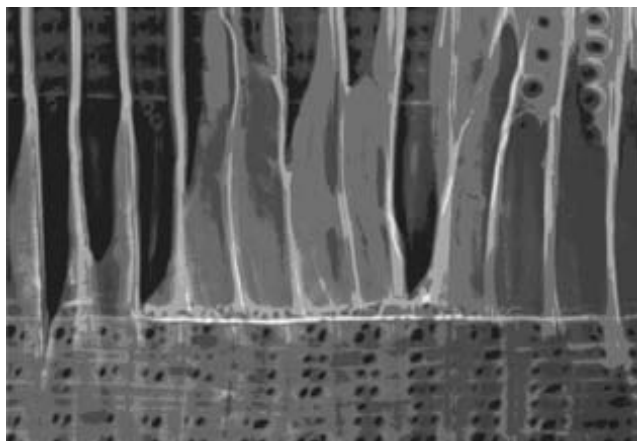

FIGURE 8.3 Radial view of tracheids of *Pinus radiata* showing radial bordered pits (upper left-hand corner) and uniseriate heterogeneous ray (center of micrograph).
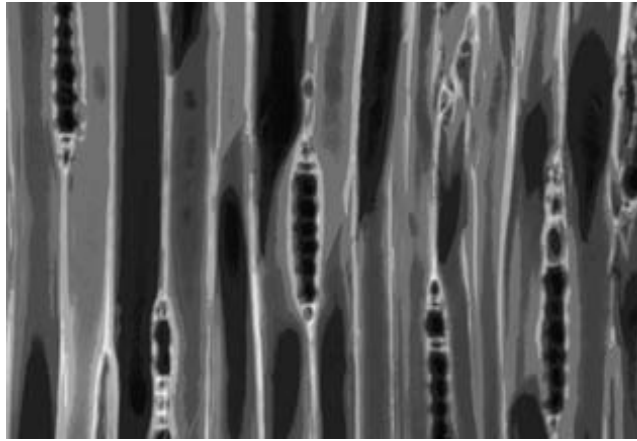
FIGURE 8.4 Tangential view of tracheids of *Pinus radiata* showing fusiform rays, and uniseriate heterogeneous and homogeneous rays.

8.2.2 SCANNING ELECTRON MICROSCOPY

The basic principle of scanning electron microscopy (SEM) is illustrated in Figure 8.5. The primary electron beam, which is produced under high vacuum at the top of the microscope by heating a metallic element, is scanned across the surface of a specimen. When the electrons strike the specimen, a variety of signals is generated, and it is the detection of specific signals that produces an image of the surface, or its elemental composition. The three signals that provide the greatest amount of information in SEM are the secondary electrons, backscattered electrons, and X-rays.
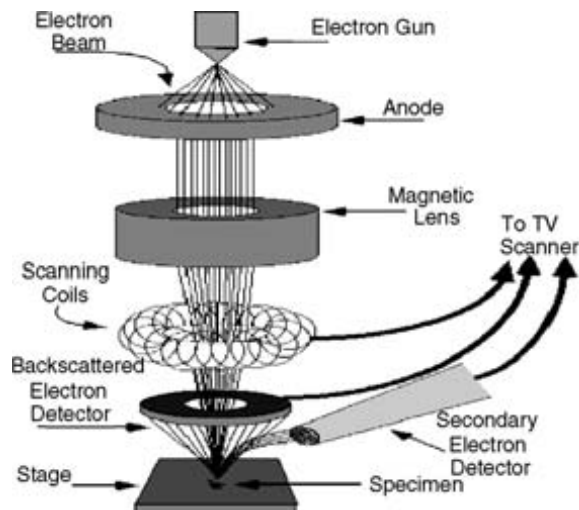
FIGURE 8.5 Principle of SEM. The primary electron beam produced at the top of the microscope by the heating of a metallic filament is focused and scanned across surface of a specimen by means of electromagnetic coils. Secondary and backscattered electron beams ejected from the surface are collected in detectors, which convert them to a signal that is processed into an image. (Courtesy of Prof. Scott Chumbley, Iowa State University, Materials Science and Engineering Department.)

Secondary electrons are emitted from the atoms occupying the top surface layer and produce an image of the surface. The contrast in the image is determined by the surface morphology. A high-resolution image can be obtained because of the small diameter of the primary electron beam.

Backscattered electrons are primary beam electrons, which are reflected by the atoms in the surface layers. The contrast in the image produced is determined by the atomic number of the elements in the surface layers. The image will therefore show the distribution of different chemical phases in the specimen surface. Because backscattered electrons are emitted from a depth in the specimen, the resolution in the image is usually not as good as for secondary electrons.

Interaction of the primary beam with atoms in the specimen causes electron shell transitions, which result in the emission of an X-ray. The emitted X-ray has an energy that is characteristic of its parent element. Detection and measurement of X-ray energy permits elemental analysis and is commonly referred to as Energy Dispersive X-ray Spectroscopy (EDS or EDX or EDXA). EDS can provide rapid qualitative, or with adequate calibration standards, quantitative analysis of elemental composition with a sampling depth of 1–2 microns. X-rays may also be used to form maps or line profiles, showing the elemental distribution in a specimen surface.

One of the latest innovations in SEM is environmental scanning microscopy (ESEM). ESEM differs from conventional SEM in two crucial aspects (Danilatos 1993, Donald 2003). First, ESEM allows the introduction of a gaseous environment in the specimen chamber although the electron gun is kept under the standard SEM high vacuum. Second, the wood specimens do not need to be coated with a metallic layer, as is the case in conventional SEM.

It should be noted that the gaseous environment in the specimen chamber plays a key role in signal detection (Danilatos 1988, Meredith et al. 1996). As the secondary electrons travel toward the positively charged detector they collide with the gas molecules. Each such collision leads to the generation of an additional daughter electron so that an amplified cascade of electrons reaches the detector. Along with additional daughter electrons, positive ions are also produced. These positive ions drift down toward the specimen, and hence serve to compensate charge build-up at the surface of non-conductive specimens such as wood. It is for this reason that non-conductive specimens do not need to be coated with a metallic layer to prevent charging artifacts and consequent loss of image quality.

Figures 8.6–8.8 show ESEM micrographs of specimens prepared from the softwood *Pinus taeda.*
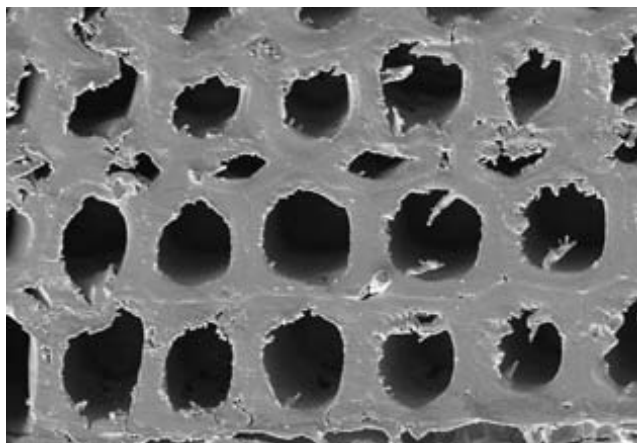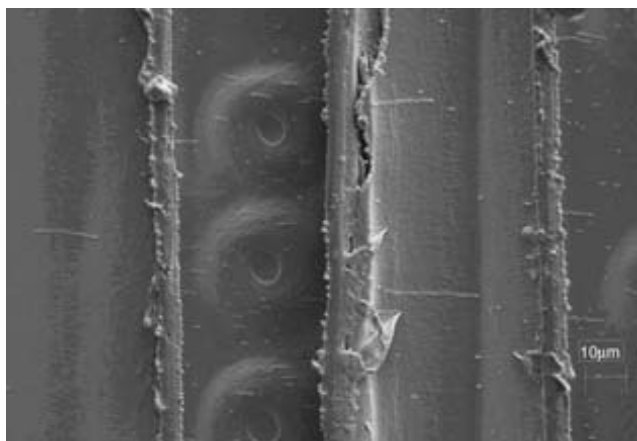

FIGURE 8.6 ESEM micrograph of the softwood *Pinus taeda* showing the transverse surface of thick-walled latewood tracheids. A uniseriate ray is visible above the bottom row of tracheids. (Courtesy T.A. Kuster, USDA Forest Service, Forest Products Laboratory, Madison, WI.)
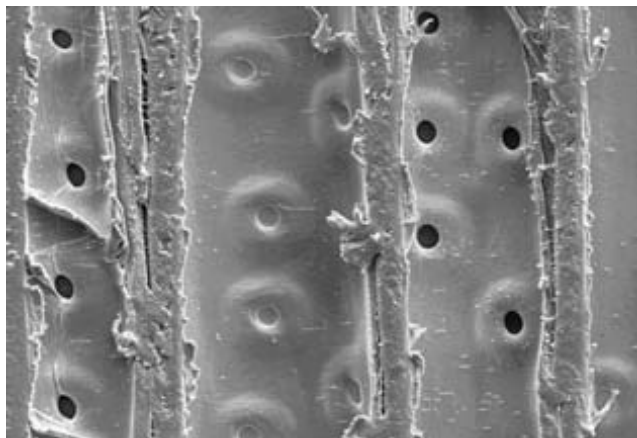
FIGURE 8.7 ESEM micrograph of the softwood *Pinus taeda* showing the radial surface of tracheids. Bordered pits are clearly visible. The warty membrane that lines the lumen is also clearly visible, especially in the left lumen where it has peeled back at some spots. (Courtesy T.A. Kuster, USDA Forest Service, Forest Products Laboratory, Madison, WI.)

8.2.3 ATOMIC FORCE MICROSCOPY

The basic principle and application of atomic force microscopy (AFM) has been the subject of a number of excellent reviews (Meyer 1992, Frommer 1992, Hoh and Engel 1993, Frisbie et al. 1994, Hanley and Gray 1994, 1995, Louder and Parkinson 1995, McGhie et al. 1995, Rynders et al. 1995, Schaefer et al 1995, Hansma et al. 1998). In atomic force microscopy (AFM), a probe consisting of a sharp tip (nominal tip radius on the order of 10 nm) located near the end of a cantilever beam is raster scanned across the surface of a specimen using piezoelectric scanners. Changes in the tip-specimen interaction are often monitored using an optical lever detection system, in which a laser is reflected off of the cantilever and onto a position-sensitive photodiode. During scanning, a particular operating parameter is maintained at a constant level, and images are generated through a feedback loop between the optical detection system and the piezoelectric scanners.


FIGURE 8.8 ESEM micrograph of the softwood *Pinus taeda* showing the tangential surface of thick-walled latewood tracheids. The tangential surface has relatively fewer bordered pits compared to the radial surface. (Courtesy T.A. Kuster, USDA Forest Service, Forest Products Laboratory, Madison, WI.)
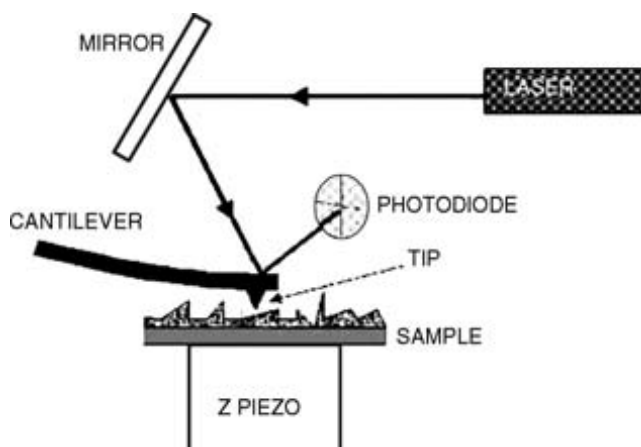
FIGURE 8.9 Schematic diagram of contact mode AFM. The tip makes soft physical contact with the sample. Optical detection of the position of the cantilever leads to a topographic map of the sample surface. (Courtesy of National Physical Laboratory, Teddington, Middlesex, UK, TW11 0LW. © Crown Copyright 2004. Reproduced by permission of the Controller of HMSO.)

Three imaging modes, contact mode, non-contact mode, and intermittent contact or tapping mode can be used to produce a topographic image of the surface. In contact mode (see Figure 8.9), the probe is essentially dragged across the surface of the specimen. During scanning, a constant bend in the cantilever is maintained. A bend in the cantilever corresponds to a displacement of the probe tip, z_t, relative to an undeflected cantilever, and is proportional to the applied normal force, $P = k \cdot z_t$, where k is the cantilever spring constant. As the topography of the surface changes, the z-scanner must move the position of the tip relative to the surface to maintain this constant deflection. Using this feedback mechanism, the topography of the specimen surface is thus mapped during scanning by assuming that the motion of the z-scanner directly corresponds to the surface topography. To minimize the amount of applied force used to scan the sample, low spring constant (k ≤ 1 N/m) probes are normally used. However, significant deformation and damage of soft samples (e.g., biological and polymeric materials) often occur during contact mode imaging in air because significant force must be applied to overcome the effects of surface roughness or adsorbed moisture as is the case with wood specimens. The combination of a significant normal force, the lateral forces created by the dragging motion of the probe tip across the specimen, and the small contact areas involved results in high contact stresses that can damage either the specimen surface, the tip, or both. To overcome this limitation, contact mode imaging can be performed under a liquid environment, which essentially eliminates problems due to surface moisture so that much lower contact forces can be used. In fact, the ability to image samples under a liquid environment is often a desirable capability of AFM, but in some cases it might not be practical or feasible. Also, working with liquid cells for many commercial AFM systems can be tricky because of the potential for spills and leaks, which can introduce liquid into the scanners.

To mitigate or completely eliminate the damaging forces associated with contact mode, the cantilever can be oscillated near its first bending mode resonance frequency (normally on the order of 100 kHz) as the probe is raster scanned above the specimen surface in either non-contact mode or tapping mode. In non-contact mode (see Figure 8.10), both the tip-specimen separation and the oscillation amplitude are on the order of 1 nm to 10 nm, such that the tip oscillates just above the specimen. The resonance frequency and amplitude of the oscillating probe decrease as the specimen surface is approached as a result of interactions with van der Waals and other long-range forces
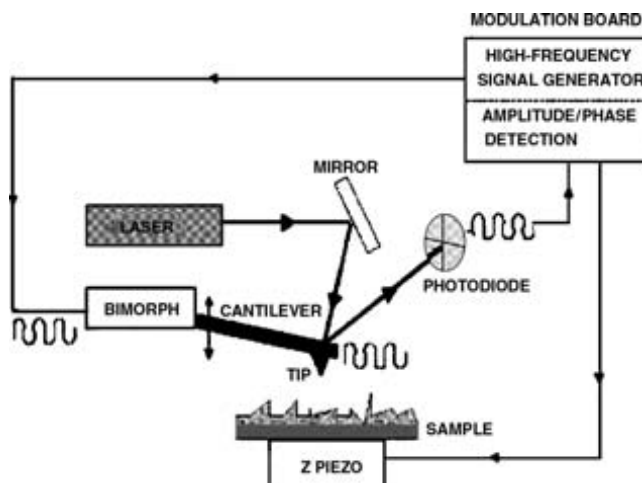
FIGURE 8.10 Schematic diagram of non-contact mode AFM. The cantilever is vibrated near the surface of the sample. Changes in the resonance frequency or vibration amplitude of the cantilever as the tip approaches the surface are used to measure changes in the sample surface topography. (Courtesy of National Physical Laboratory, Teddington, Middlesex, UK, TW11 0LW. © Crown Copyright 2004. Reproduced by permission of the Controller of HMSO.)

extending above the surface. These types of forces tend to be quite small relative to the repulsive forces encountered in contact mode. Both a constant amplitude or constant resonance frequency is maintained through a feedback loop with the scanner, and, similar to contact mode, the motion of the scanner is used to generate the topographic image. To reduce the tendency of the tip to be pulled down to the surface by attractive forces, the cantilever spring constant is normally much higher compared to contact mode cantilevers. The combination of weak forces affecting feedback and large spring constants causes the non-contact AFM signal to be small, which can lead to unstable feedback and requires slower scan speeds than either contact mode or tapping mode. Also, the lateral resolution in non-contact mode is limited by the tip-specimen separation and is normally lower than that in either contact mode or tapping mode.

Tapping mode tends to be more applicable to general imaging in air, particularly for soft samples, as the resolution is similar to contact mode while the forces applied to the specimen are lower and less damaging. In fact, the only real disadvantages of tapping mode relative to contact mode are that the scan speeds are slightly slower and the AFM operation is a bit more complex, but these disadvantages tend to be outweighed by the advantages. In tapping mode, the cantilever oscillates close to its first bending mode resonance frequency, as in non-contact mode. However, the oscillation amplitude of the probe tip is much larger than for non-contact mode, often in the range of 20 nm to 200 nm, and the tip makes contact with the sample for a short time in each oscillation cycle. As the tip approaches the specimen, the tip-specimen interactions alter the amplitude, resonance frequency, and phase angle of the oscillating cantilever. During scanning, the amplitude at the operating frequency is maintained at a constant level, called the *set-point amplitude*, by adjusting the relative position of the tip with respect to the specimen. In general, the amplitude of oscillation during scanning should be large enough for the probe to maintain enough energy to allow the tip to tap through and back out of the surface layer.

One recent development in tapping mode is the use of the changes in phase angle of the cantilever probe to produce a second image, called a phase image or phase contrast image. This image often provides significantly more contrast than the topographic image and has been shown to be sensitive to material surface properties, such as stiffness, viscoelasticity, and chemical

composition. In general, changes in phase angle during scanning are related to energy dissipation during tip-sample interaction and can be caused by changes in topography, tip-specimen molecular interactions, deformation at the tip-specimen contact, and even experimental conditions. Depending on the operating conditions, different levels of tapping force might be required to produce an accurate and reproducible image of a surface. Also, the amount of tapping force used will often affect the phase image, particularly with regard to whether local tip-specimen interactions are attractive or repulsive.

Similar contrast images can be constructed concurrently with the topographic image in contact mode. One example is lateral force or friction force imaging, in which torsional rotation of the probe is detected while the probe is dragged across the surface in a direction perpendicular to the long axis of the cantilever. Friction force imaging with a chemically modified probe (i.e., a probe that has been coated with a monolayer of a specific organic group) is often referred to as chemical force microscopy. Another example of contrast imaging is force modulation, which combines contact mode imaging with a small oscillation of the probe tip at a frequency far below resonance frequency. This oscillating force should deform softer regions more than harder regions of a heterogeneous sample so that contrast between these regions is observed. In practice, however, the difference between the elastic modulus of the different regions usually has to be substantial (e.g., rubber particles in a plastic, carbon fibers in an epoxy) for contrast to be realized. Thus far, these types of AFM contrast images are purely qualitative as a result of inaccurate or unknown spring constants, unknown contact geometry, and contributions from different types of surface properties.

Figure 8.11 shows topographic (height) and phase contrast images of a bordered pit on the surface of the cell wall of a softwood specimen. The images were acquired and recorded simultaneously by tapping-mode AFM at ambient conditions, using a Nanoscope MultiMode SPM™.

0		3.00 µm 0		3.00 µm
Data type 2 range	Height 200.0 nm	Data type 2 range	Phase 25.00 de	
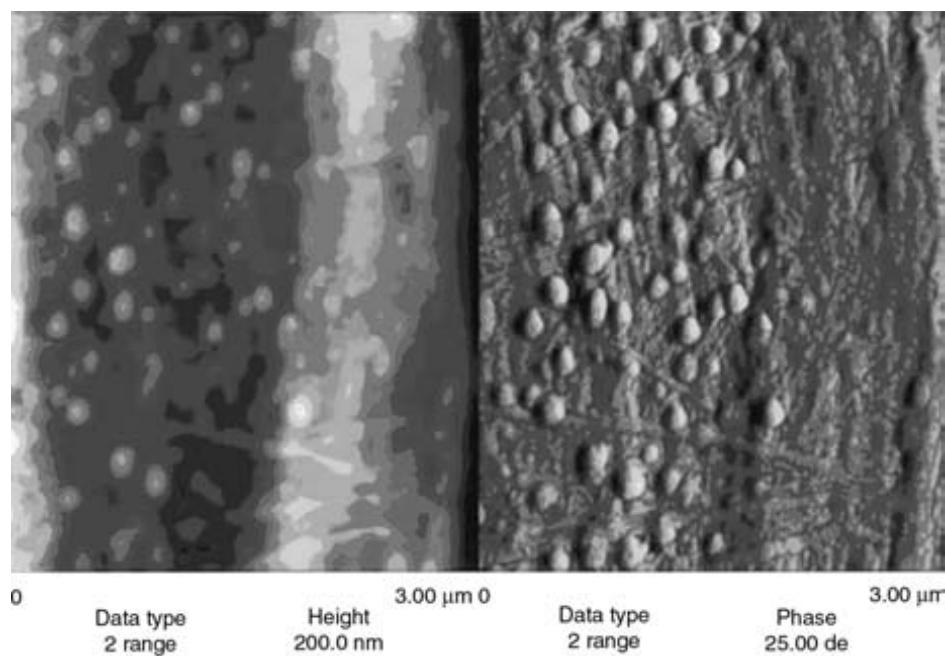
FIGURE 8.11 Topographical (height) and phase contrast images of a bordered pit showing the fibrillar morphology of the margo. The phase contrast image clearly shows the network of nanofibrils that constitute the margo, and nodules located close to the pores that permeate the margo.

8.3 SPECTROSCOPIC METHODS FOR CHARACTERIZING SURFACE PROPERTIES

Although a broad array of spectroscopic methods for surface analysis of materials exists, only a handful of these have been applied in the characterization of wood surfaces. The focus of this section will be on those methods that the author deemed to be of greatest interest.

Spectroscopic methods can be divided into three classes: molecular, electronic, and mass spectroscopies. Molecular spectroscopy includes Fourier transform infrared (FTIR), Fourier transform attenuated total reflectance infrared (FT-ATR), and Fourier Transform Raman (FT-Raman). Electronic spectroscopy includes X-ray photoelectron (XPS) and energy dispersive X-ray spectroscopy (EDXA, EDX or EDS). Mass spectroscopy includes secondary ion mass spectroscopy (SIMS) and static secondary ion mass spectroscopy (SSIMS).

8.3.1 Molecular Spectroscopy

Molecular spectroscopic methods can provide information about the chemical composition of a surface. However, successful characterization of a wood surface by any of the molecular spectroscopic techniques depends upon a judicious choice of sampling techniques and critical interpretation of the data. Detailed descriptions of the fundamentals and applications of molecular spectroscopy can be found elsewhere (Mirabella 1998, Stuart 2004). As significant advances in instrumentation are realized, new applications of infrared spectroscopy in surface characterization of wood have emerged.


TABLE 8.1
Assignment of IR Bands of Solid Wood or Wood Particles Measured by Diffuse Reflectance FTIR

Band Position, cm^{-1}	Assignment
3380 (3418)[a]	O-H stretch vibration (bonded)
2928 (2928)	C-H stretch vibration
1736 (1745)	C=O stretch vibration (unconjugated)
1655 (1660)	H-O-H deformation vibration of adsorbed water and conjugated C=O stretch vibration
1595 (1596)	Aromatic skeletal and C=O stretch vibration
1504 (1507)	Aromatic skeletal vibration
1459 (1465)	C-H deformation (asymmetric) and aromatic vibration in lignin
1423 (1427)	C-H deformation (asymmetric)
1372 (1374)	C-H deformation (symmetric)
1326 (1329)	-CH$_2$ wagging vibration in cellulose
1267 (1270)	C-O stretch vibration in lignin, acetyl and carboxylic vibration in xylan
1236 (1242)	C-O stretch vibration in lignin, acetyl and carboxylic vibration in xylan
1158 (1165)	C-O-C asymmetric stretch vibration in cellulose and hemicellulose
1113 (1128[b])	O-H association band in cellulose and hemicellulose
1055[b] (1083)	C-O stretch in cellulose and hemicellulose
1042 (1036)	C-O stretch
1000 (1003)	C-O stretch in cellulose and hemicellulose
897 (899)	C1 group frequency in cellulose and hemicellulose
667 (670)	C-O-H out-of-plane bending mode in cellulose

[a] Quantities given in parenthesis correspond to band positions obtained from solid wood chips or wood particles undiluted with KBr.
[b] Highest intensity band

Source: Pandey and Theagarajan 1997.
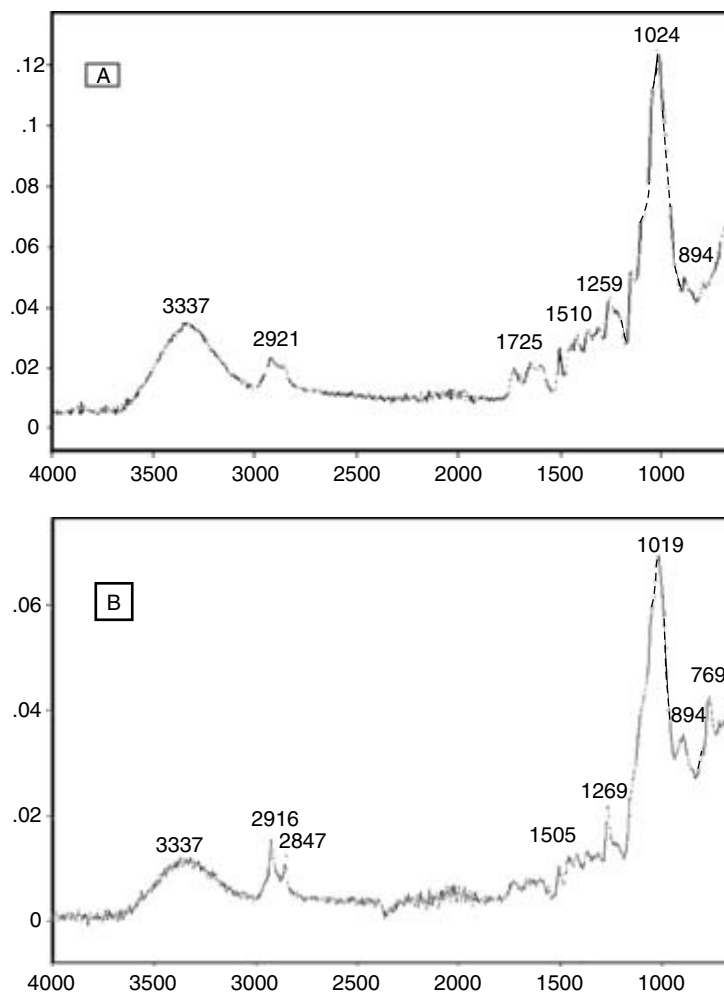
FIGURE 8.12 FTIR-ATR spectra of a wood wafer before (A) and after (B) coating with a thin film of alkoxysilanes.

FTIR and FT-ATR spectra of wood samples have been reported in the literature (Deshmukh and Aydil 1996, Tshabalala et al. 2003). Assignment of infrared absorption bands measured by different FTIR techniques is given in Table 8.1. Figure 8.12 shows examples of infrared spectra of the surface of a softwood wafer obtained by FTIR-ATR.

Infrared analysis of wood surfaces is generally not considered to be sufficiently surface sensitive because the sampling depth of infrared radiation is in the order of 100 μm. Consequently, changes in infrared spectral features caused by changes in surface chemistry are often masked by the spectral features of the underlying bulk chemistry of the wood specimen. In the example shown in Figure 8.12(B), the peaks at 2916, 2847, 1269, 894, and 769 cm^{-1} were attributed to the alkoxysilane thin film that was deposited on the wood wafer (Tshabalala et al. 2003). The peaks at 2916 and 2847 cm^{-1} were assigned to the asymmetric and symmetric C-H stretch modes of the –CH$_3$ and –CH$_2$ groups (Sali et al. 1994, Deshmukh and Aydil 1996, Conley 1996); the peak at 1269 cm^{-1} was assigned to the Si-CH$_3$ bending mode, and the peaks at 894 and 769 cm^{-1} were assigned to Si-C, Si-O and Si-O-CH$_3$ groups (Selamoglu et al. 1989, Fracassi et al. 1992, Libermann and Lichtenberg 1994, Conley 1996).

TABLE 8.2
Raman Band Assignment in the Spectra of Softwood Cellulose and Lignin

Band Position cm^{-1}	Assignment	Attributed to
3065 m[a]	Aromatic stretch	lignin
3007 sh	C-H stretch in OCH$_3$, asymmetric	lignin
2938 m	C-H stretch in OCH$_3$, asymmetric	lignin
2895 vs	C-H and CH$_2$ stretch	cellulose
2886 sh	C-H stretch in R$_3$C-H	lignin
2848 sh	C-H and CH$_2$ stretch	cellulose
2843 m	C-H stretch in OCH$_3$, symmetric	lignin
1658 s	Ring conj. C=C stretch of coniferyl alcohol; C=O stretch of coniferylaldehyde	lignin
1620 sh	Ring conjugated C=C stretch of coniferylaldehyde	lignin
1602 vs	Aryl ring stretch, symmetric	lignin
1508 vw	Aryl ring stretch, asymmetric	lignin
1456 m	H-C-H and H-O-C bending	cellulose
1454 m	O-CH$_3$ deformation; CH$_2$ scissoring; guaiacyl ring vibration	lignin
1428 w	O-CH$_3$ deformation; CH$_2$ scissoring; guaiacyl ring vibration	lignin
1393 sh	Phenolic O-H bend	lignin
1377 m	H-C-C, H-C-O and H-O-C bending	cellulose
1363 sh	C-H bend in R$_3$C-H	lignin
1333 m	Aliphatic O-H bend	lignin
1298 sh	H-C-C and H-C-O bending	cellulose
1297 sh	Aryl-O of aryl-OH and aryl-O-CH$_3$; C=C stretch of coniferyl alcohol	lignin
1271 m	Aryl-O of aryl-OH and aryl-O-CH$_3$; guaiacyl ring (with C=O group)	lignin
1216 vw	Aryl-O of aryl-OH and aryl-O-CH$_3$; guaiacyl ring (with C=O group)	lignin
1191 w	A phenol mode	lignin
1149 sh	C-C and C-O stretch plus H-C-C and H-C-O bending	cellulose
1134 m	A mode of coniferaldehyde	lignin
1123 s	C-C and C-O stretch	cellulose
1102 w	Out of phase C-C-O stretch of phenol	lignin
1095 s	C-C and C-O stretch	cellulose
1073 sh	C-C and C-O stretch	cellulose
1063 sh	C-C and C-O stretch	cellulose
1037 sh	C-C and C-O stretch	cellulose
1033 w	C-O of aryl-O-CH$_3$ and aryl-OH	lignin
1000 vw	C-C and C-O stretch	cellulose
971 vw	C-C and C-O stretch	cellulose
969 vw	-C-C-H and –HC=CH- deformation	lignin
926 vw	-C-C-H wag	lignin
900 vw	Skeletal deformation of aromatic rings, substituent groups and side chains	lignin
899 m	H-C-C and H-C-O bending at C6	cellulose
787 w	Skeletal deformation of aromatic rings, substituent groups and side chains	lignin
731 w	Skeletal deformation of aromatic rings, substituent groups and side chains	lignin
634 vw	Skeletal deformation of aromatic rings, substituent groups and side chains	lignin
591 vw	Skeletal deformation of aromatic rings, substituent groups and side chains	lignin
555 vw	Skeletal deformation of aromatic rings, substituent groups and side chains	lignin
537 vw	Skeletal deformation of aromatic rings, substituent groups and side chains	lignin
520 m	Some heavy atom stretch	cellulose
491 vw	Skeletal deformation of aromatic rings, substituent groups and side chains	lignin
463 vw	Skeletal deformation of aromatic rings, substituent groups and side chains	lignin
458 m	Some heavy atom stretch	cellulose

TABLE 8.2
Raman Band Assignment in the Spectra of Softwood Cellulose and Lignin (*Continued*)

Band Position cm^{-1}	Assignment	Attributed to
435 m	Some heavy atom stretch	cellulose
384 w	Skeletal deformation of aromatic rings, substituent groups and side chains	lignin
380 m	Some heavy atom stretch	cellulose
357 w	Skeletal deformation of aromatic rings, substituent groups and side chains	lignin
351 w	Some heavy atom stretch	cellulose

[a]*Note:* vs = very strong; s = strong; m = medium; w = weak; vw = very weak; sh = shoulder. Band intensities are relative to other peaks in the spectrum.

Source: Agarwal 1999.

Raman and infrared spectra give basically the same kind of molecular information, and both methods can be used to supplement or complement each other. Although Raman spectra are theoretically simpler than the corresponding infrared spectra, primarily because overlapping bands are much less common in Raman spectroscopy, its use in the study of wood surfaces is not widespread. The primary reason for this lack of popularity has been the difficulty of obtaining sufficiently intense Raman bands, which are not completely masked by the fluorescence bands emitted by the wood components when irradiated with visible light. However, with the advent of FT-Raman and the introduction of the red laser source (excitation wavelength, 1064 nm), this difficulty has been largely overcome, and application of FT-Raman to the study of wood surfaces is likely to increase.

FT-Raman spectra of wood and wood components have been reported in the literature (Agarwal and Ralph 1997, Agarwal 1999). Table 8.2 gives a summary of band assignment in the FT-Raman spectra of wood components.
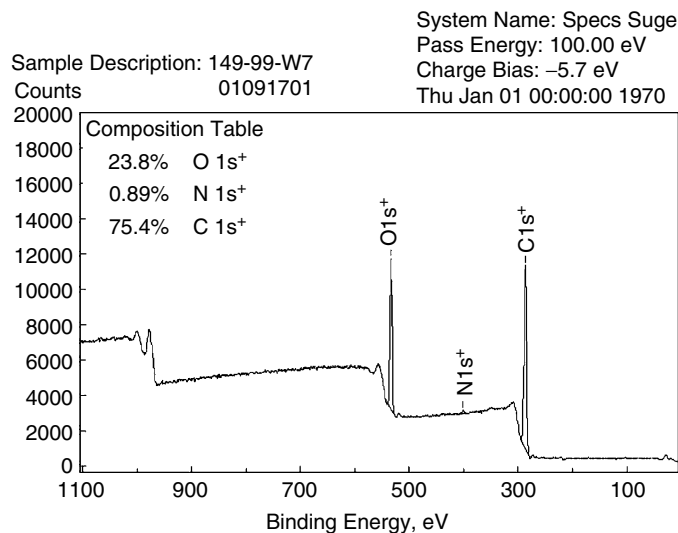
8.3.2 ELECTRON SPECTROSCOPY

Electron spectroscopy is concerned with the energy analysis of low energy electrons (generally in the range of 20-2000 eV) liberated from the surface of a specimen when it is irradiated with soft X-rays or bombarded with an electron beam (Watts 1990). Two methods of electron spectroscopy have been developed: X-ray photoelectron spectroscopy (XPS), also known as electron spectroscopy for chemical analysis (ESCA), and Auger electron spectroscopy (AES). Since AES has not been applied to the study of wood surfaces, the rest of this discussion will focus on XPS, which has been widely used for the characterization of the elemental composition of wood surfaces.

In XPS, the surface of a sample maintained in a high vacuum ($10^{-6} - 10^{-11}$ torr) is irradiated with X-rays, usually from a Mg or Al anode, which provide photons of 1253.6 eV and 1486.6 eV, respectively. Electrons are ejected from the core levels of atoms in the surface, and their characteristic binding energies are determined from the kinetic energy of the ejected electrons and the energy of the incident x-ray beam.

The kinetic energy (E_K) of the electron is the experimental quantity measured by the spectrometer. The binding energy of the electron (E_B) of the electron is related to the experimentally measured kinetic energy by the following relationship:

$$E_B = h\nu - E_K - W \tag{8.1}$$

where $h\nu$ is the incident photon energy and W is the spectrometer work function.

System Name: Specs Suge
Pass Energy: 100.00 eV
Charge Bias: −5.7 eV
Thu Jan 01 00:00:00 1970

Sample Description: 149-99-W7
Counts   01091701

Composition Table

23.8%   O 1s$^+$

0.89%   N 1s$^+$
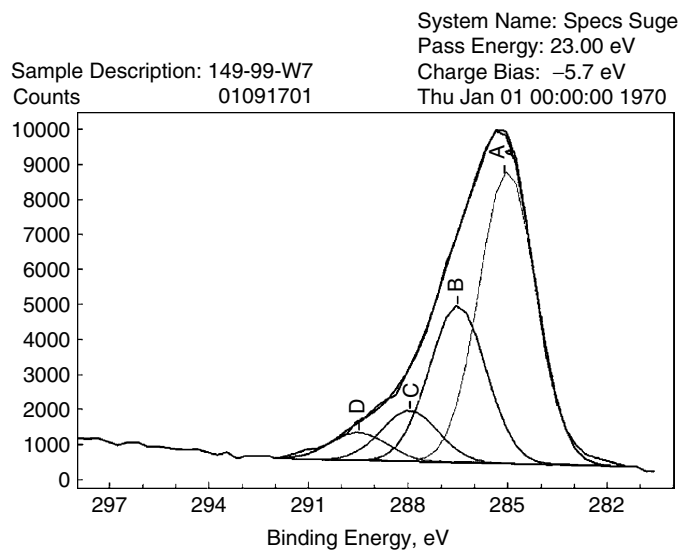
75.4%   C 1s$^+$

Binding Energy, eV

FIGURE 8.13 XPS survey spectrum of a wood specimen of *Pinus taeda* shows the elemental composition of the surface.

The kinetic energy of the electrons ejected from the surface of a specimen is determined by means of an analyzer that gives a photoelectron spectrum. The photoelectron spectrum gives an accurate representation of the electronic structure of an element, as all electrons with a binding energy less than the incident photon energy will be featured in the spectrum.

The characteristic binding energy of a given atom is also influenced by its chemical environment. This dependence allows the assignment of a given atom to a particular chemical functional group on the surface. The sampling depth of XPS is about 5–10 nm.

Examples of survey and high-resolution XPS spectra of a wood specimen are shown in Figures 8.13 and 8.14, respectively. The survey spectrum gives the surface elemental composition

System Name: Specs Suge
Pass Energy: 23.00 eV
Charge Bias: −5.7 eV
Thu Jan 01 00:00:00 1970

Sample Description: 149-99-W7
Counts   01091701

Binding Energy, eV

FIGURE 8.14 High-resolution XPS spectrum of the C1$_{s*}$ carbon showing the existence of different states or classes of carbon atoms on the surface of the wood specimen (A = C1; B = C2; C = C3; and D = C4).

of the wood specimen. As expected, the spectrum is dominated by carbon and oxygen peaks, which are the elements that make up the constituents of wood. The high-resolution spectrum of the carbon peak shows the presence of different chemical states, or classes, of carbon on the wood surface.

In early studies on the surface analysis of paper and wood fibers by XPS, C1s and O1s spectra were obtained for samples of Whatman™ filter paper, bleached kraft and bleached sulfite paper, spruce dioxane lignin, stone groundwood pulp, refiner mechanical pulp, and thermomechanical pulp.

The C1s peak was observed to consist of four main components, which were ascribed to four classes of carbon atoms present in wood components. Class I carbon atoms are those bonded to carbon or hydrogen; Class II carbon atoms are bonded to a single non-carbonyl oxygen atom; Class III carbon atoms are bonded to two non-carbonyl or to a single carbonyl oxygen atom, and Class IV carbon atoms are ascribed to the carboxyl carbon. The four components were designated C1, C2, C3, and C4, respectively. The change in the relative magnitude of these components as a function of the oxygen ratio was taken to suggest that both lignin and extractives contribute to the ongoing change in surface composition from pure cellulose to mechanical wood pulps (Dorris and Gray 1978a,b, Gray 1978).

In another pioneer study on the applicability of XPS to the chemical surface analysis of wood fibers, the oxygen-to-carbon (O/C) ratio of wood and wood fibers prepared by different methods was determined. The deviation of the observed O/C ratios from theoretical values was used to provide qualitative characterization of the surface chemical composition. For example, samples of unextracted and extracted pine chips showed O/C ratios of 0.26 and 0.42, respectively. This was interpreted as indicative of surfaces rich in lignin because the observed ratios were very close to the theoretical values of 0.33–0.36 calculated for spruce lignin and considerably lower than the theoretical value of 0.83 for cellulose (Mjörberg 1981).

In a number of studies, the XPS technique has been applied for monitoring the modification of wood surfaces. Wood surfaces treated with aqueous solutions of nitric acid and sodium periodate were analyzed by XPS, and it was observed that the periodate treatment led to a dramatic increase in the relative magnitude of the C2 component. The nitric acid treatment, on the other hand, led to the appearance of a C4 component and a significant increase of the C3 component at the expense of a decrease in both the C1 and C2 components (Young et al. 1982). In another study, XPS data of wood and cellulose surfaces treated with aqueous chromium trioxide showed that at least 75% of Cr(VI) was reduced to Cr(III), and the C1s spectra showed that the surface concentration of hydroxyls decreased, while the hydrocarbon component increased. It was suggested that this change occurred through oxidation of primary alcohols in the cellulose to acids, followed by decarboxylation, and that there were possible cellulose-chromium interactions in addition to the previously proposed chromium-lignin interactions (Williams and Feist 1984).

Changes in the surface chemical composition of solid residues of quaking aspen (*Populus tremuloides*) wood, extracted with supercritical fluid methanol, were monitored by XPS, and it was shown that the C1s peak provided information that allowed for the rapid measurement of the proportion of carbon in polyaromatics. The components of the O1s peak were also tentatively assigned to oxygens in the major wood components and to minor extractives, recondensed material, and strongly adsorbed water (Ahmed et al. 1987, Ahmed et al. 1988). In another XPS study of weathered and UV-irradiated wood surfaces, the observed increase in the O/C ratio was interpreted as an indication of a surface rich in cellulose and poor in lignin (Hon 1984, Hon and Feist 1986).

The surface composition of grafted wood fibers has also been characterized by XPS. By grafting poly(methylmethacrylate) onto wood fibers, this study demonstrated the possibility of tailoring the chemical surface composition of the wood fiber for specific end uses in thermoplastic composites (Kamdem et al. 1991).

The XPS technique has also been applied to the study of the surface composition of wood pulp prepared by the steam explosion pulp (SEP), conventional chemimechanical pulp (CMP) and conventional chemithermomechanical pulp (CTMP) processes (Hua et al. 1991, Hua et al. 1993a, b). Based on the theoretical O/C ratios and C1 contents of the main components of the wood fibers

(i.e., carbohydrates, lignin and extractives), a ternary diagram was constructed to illustrate the relative amounts of the three components on the surface. A tentative assignment of two components of the oxygen 1s peak, O1 and O2, was also made. The O1 component, which has a lower binding energy, was assigned to the oxygen in lignin, and O2 was assigned to the oxygen in the carbohydrates. The investigators suggested that the percentage of the O1 peak area could be viewed as a measure of the lignin on the fiber surface.

8.3.3 Mass Spectroscopy

Surface mass spectroscopy techniques consist of measuring the masses of secondary ions that are ejected, in a process known as sputtering, from the surface of a specimen when a primary beam of energetic particles bombards it. The secondary ions can provide unique information about the chemistry of the surface from which they originated. Thus, surface mass spectroscopy and surface electron spectroscopy complement each other. Indeed, it is common practice to use electron spectroscopy in combination with surface mass spectroscopy to characterize the surface chemistry of an unknown specimen.

Three main methods of surface mass spectroscopy are commonly used: secondary ion mass spectrometry (SIMS), laser ionization mass spectrometry (LIMA), and sputtered neutral mass spectrometry (SNMS). However, SIMS is by far the most commonly used surface mass spectroscopic techniques. While SIMS always revolves around the sputtering process, different modes of operation of SIMS exist. The three main modes of operation are static, dynamic, and scanning (or imaging) SIMS (Johnson and Hibbert 1992).

Static SIMS (SSIMS) operates under gentle bombardment conditions and provides information about the chemistry of the upper surface of a specimen, while causing negligible surface damage. Dynamic SIMS (DSIMS) operates under relatively harsher bombardment conditions and provides information about the chemistry of a surface from a few nanometers to several hundred microns in depth. Scanning or imaging SIMS, using highly focused ion beams, provides detailed chemical images with spatial resolution approaching that associated with scanning electron microscopy (less than 100 nm).

In SSIMS, the surface of a sample maintained in a high vacuum (10^{-6}–10^{-11} torr) is bombarded with ions (Ar^+, Xe^+, Cs^+ or Ga^+) at well-defined energies in the range of 1–4 KeV. Secondary ions are sputtered from the surface and are detected in a mass spectrometer. To keep depletion of the surface to a minimum, the primary current is held at approximately 1 nA/cm^2. Under these conditions, only a very small fraction (approximately 1%) of the uppermost monolayer is consumed. The relatively low secondary ion flux is typically detected and analyzed in a time-of-flight mass spectrometer (TOFMS). The TOFMS has high sensitivity, extended mass range, and high mass resolution, and is applicable to virtually all fields of science and technology where solid surfaces and their behavior are important (Wattws 1992, Winogard 1993, Benninghoven et al. 1993, Comyn 1993, Li and Gardella 1994,).

The development of SIMS and its application in the study of paper surfaces is the subject of an excellent review by Detter-Hoskin and Busch (1995). Although SSIMS spectra are complicated and sometimes difficult to interpret, the SSIMS technique has been successfully applied in the study of the surface composition and topochemistry of paper surfaces. Brinnen compared the information content of XPS and SSIMS for characterizing sized paper surfaces. He observed that while XPS readily detected the presence of sizing agents, it provided little structural information. TOF-SSIMS, on the other hand, could be used to identify the chemical structures. Brinen also showed that the spatial distribution of the sizing agents on the paper surfaces could be obtained using TOF- SSIMS (Brinen 1993). In a combination of XPS, TOF-SIMS, and paper chromatography, Brinen et al studied the cause of sizing difficulties in sulfite paper. Using SIMS imaging, they observed concentrated islands of pitch, which were implicated in the desizing effect (Brinen and Kulick 1995).

In another study of paper surfaces, Pachuta and Staral demonstrated that TOF-SSIMS, with its extended mass range and high sensitivity, was a useful tool for the nondestructive analysis of
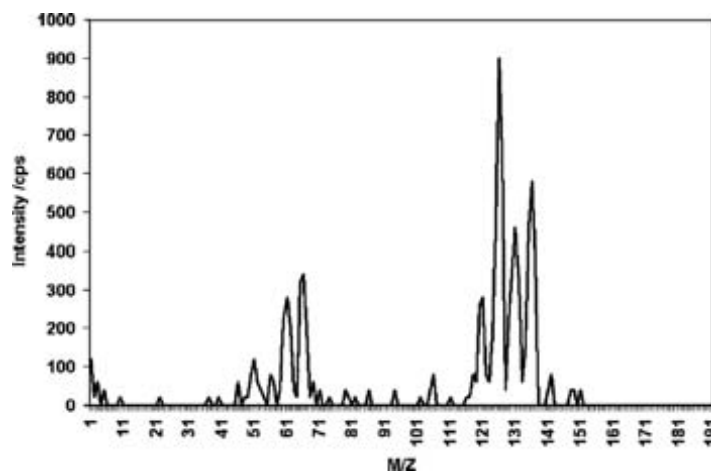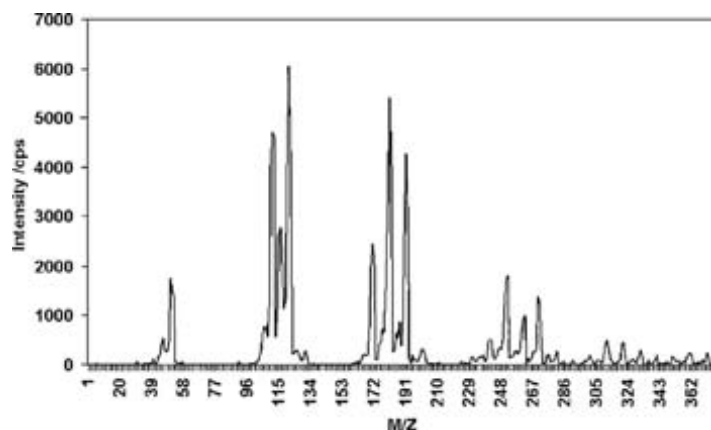
FIGURE 8.15 SSIMS positive ion spectrum of a wood specimen acquired on a MiniSIMS™ desktop chemical microscope (Millbrook Instruments, Ltd.).

colorants on paper. They observed that the use of SSIMS conditions produced no detectable alteration of the paper samples (Pachuta and Staral 1994).

SIMS has also been used in the imaging of fiber surfaces. Tan and Reeve used SIMS imaging to reveal the micro distribution of organochlorine on fully bleached pulp fibers. They observed that pulp-bound chlorine was present over the entire surface and throughout the fiber cross-section. On the fiber's outer surface, the chlorine concentration was observed to be higher in some small areas. In cross-section, chlorine was observed to be concentrated in the middle of the secondary wall. They concluded that, since most of the pulp bound organochlorine is covalently linked to large carbohydrate molecules held deep within the fiber wall, it was not likely to diffuse out of the fiber even after a long time (Tan and Reeve 1992).

SSIMS spectral libraries are still at the early stages of development, and as more spectra of biomaterials, including lignocellulosic materials are added to the libraries, SSIMS will become a very productive technique for characterizing the surface chemistry of wood and wood composites. Figure 8.15 shows a SSIMS positive ion spectrum of the surface a wood specimen, and Figure 8.16

FIGURE 8.16 SSIMS positive ion spectrum of a wood specimen coated with a thin film of alkoxysilanes acquired on a MiniSIMS™ desktop chemical microscope (Millbrook Instruments, Ltd.).

shows a SSIMS positive ion spectrum of the surface of the same wood specimen after coating it with a thin film of alkoxysilanes. Although the peaks were not assigned, the effect of the coating on the surface chemistry of the wood specimen is clearly evident from the appearance of additional peaks (M/Z = 111, 116, 121, 171, 181, 191, 242, 252, 262, and 270).

8.4   THERMODYNAMIC METHODS FOR CHARACTERIZING SURFACE PROPERTIES

Over the years, two methods for determining the surface thermodynamic properties (surface energy and acid-base characteristics) of wood have been developed. The first method, which is known as contact angle analysis (CAA), is based on wetting the wood surface with a liquid. The second technique, which is known as inverse gas chromatography (IGC), is based on the adsorption of organic vapors on the wood surface. Another major difference between the two methods is that solid samples for IGC analysis should be in a finely divided form, while samples for CAA can be in any form, including small coupons or wafers.

8.4.1   CONTACT ANGLE ANALYSIS

There are two approaches to contact angle analysis (CAA): static and dynamic contact angle measurements. In static CAA the liquid-solid angle of a sessile drop of liquid on the surface of a wood specimen is observed and measured by means of contact angle meter. The contact angle, θ, of a drop of liquid on the surface of a specimen is shown schematically in Figure 8.17. The cosine of the contact angle ($\cos \theta$) is related to the surface energy of the specimen by the Young equation (Nguyen and Johns 1978).

$$\gamma_{LV}\cos \theta = \gamma_{SV} - \gamma_{SL} = \gamma_S - \gamma_{SL} - \pi_e \tag{8.2}$$

where γ_S is the surface energy of a solid measured in vacuum, γ_{SL} and γ_{SV} are the surface-free energies on the interface between solid and liquid and of the solid and saturated vapor, respectively; γ_{LV} is the surface tension of the liquid against its vapor; and π_e is the equilibrium spreading pressure of the adsorbed vapor of the liquid on solid and is defined as:

$$\pi e = \gamma_S - \gamma_{SV} \tag{8.3}$$

There are only two quantities in Equation 8.2 that can be determined experimentally: γ_{LV} and $\cos \theta$. The surface tension of the liquid, γ_{LV} and $\cos \theta$, can be measured by several methods
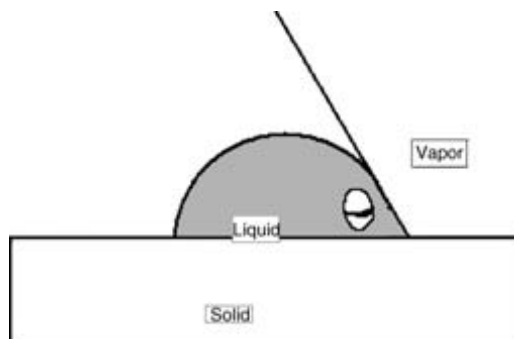

FIGURE 8.17 Schematic diagram of the contact angle, θ at the solid-liquid interface.

(Adamson 1967), but contact angle θ can only be obtained when the surface tension of the liquid is higher than the surface-free energy of the solid (assuming that γ_{SL} and π_e in Equation 8.2 are approximately equal to zero). In that case, the surface energy of the solid can be estimated from Equation 8.4:

$$\gamma_S \cong \gamma_{LV} \, \mathrm{Cos} \, \theta \qquad\qquad (8.4)$$

Zisman (Adamson 1967) introduced the well-known empirical approach to estimate the surface-free energy of a solid by plotting the cosine of the contact angle θ versus the surface tension of a series of liquids of known surface tension. The point at which the resulting straight line plot intercepts the horizontal line, Cos $\theta = 1$ (zero contact angle), is called the critical surface tension, γ_C. Zisman's plot is generally described by the following equation:

$$\mathrm{Cos} \, \theta = 1 + b(\gamma_C - \gamma_{LV}) \qquad\qquad (8.5)$$

where b is the slope of the line. Zisman's critical surface tension provides one of the most convenient means of expressing the surface energy of a solid.

In dynamic CAA, the contact angle is measured by means of a dynamic contact angle analyzer, which consists of a precision balance for measuring the wetting force exerted on a specimen as it is dipped and withdrawn from a liquid of known surface tension, γ_{LV}. As shown in the schematic diagram in Figure 8.18, the weight of the solid specimen is recorded by means of a precision balance as it is immersed and withdrawn from the liquid. Immersion and withdrawal of the specimen is accomplished by raising or lowering a cup of liquid placed on motorized elevator. The immersion graph, which is also known as a hysteresis loop, is captured by a data system that is interfaced to the control system of the dynamic contact angle analyzer. The immersion graph is essentially a plot of the measured wetting force versus the immersion depth of the specimen.
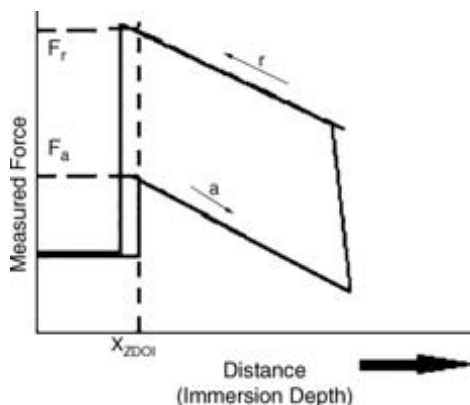
The wetting force is related to the contact angle by the following equation:

$$F = \gamma_{LV} \, \mathrm{PCos} \, \theta \qquad\qquad (8.6)$$

where F is the wetting force, γ_{LV} is the surface tension of the liquid, and P is the wetted perimeter of the solid specimen.
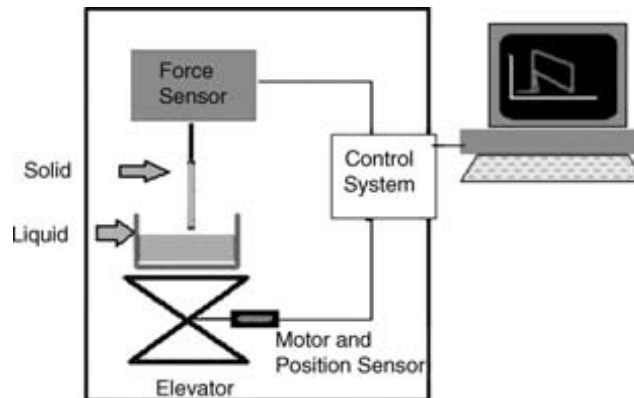
FIGURE 8.18 Schematic diagram of a Dynamic Contact Angle Analyzer.

FIGURE 8.19 Schematic diagram of the immersion graph as the specimen is immersed (a) and withdrawn (r) from the liquid. The vertical broken line coincides with the point when the specimen first comes into contact with the liquid at the zero depth of immersion, $x = X_{ZDOI}$.

As shown in Figure 8.19, the advancing and receding contact angles can be calculated from the advancing wetting force F_a and the receding wetting force F_r by the following equations:

$$\text{Cos } \theta_a = F_a/\gamma_{LV} \, P \qquad (8.7)$$

$$\text{Cos } \theta_r = F_r/\gamma_{LV} \, P \qquad (8.8)$$

F_a and F_r are located on the immersion graph at the points of intersection of the vertical line drawn through $x = X_{ZDOI}$ and the advancing line (a) and receding line (r) respectively.

The surface energy of the solid can be estimated by combining Equation 8.4 with Equation 8.7 or Equation 8.8; hence,

$$\gamma_S \cong F_a/P \qquad \text{or} \qquad \gamma_S \cong F_r/P \qquad (8.9)$$

8.4.2 INVERSE GAS CHROMATOGRAPHY

Inverse gas chromatography (IGC) involves packing the material to be studied, typically of a fibrous or particle form, into the column of a gas chromatograph. The retention behavior of a known vapor probe, which is injected into the carrier gas that passes through the packed column, allows the solid-vapor adsorption characteristics, and thus the surface thermodynamic properties, of the material to be quantified (Shultz and Lavielle 1989, Fowkes 1990, Kamdem and Reidl 1991, Lavielle and Schultz 1991, Felix and Gatenhholm 1993, Kamdem et al. 1993, Farfard et al. 1994, Williams 1994, Chtourou et al. 1995, Belgacem 2000).

The key parameter in IGC measurements is the specific retention volume, $V_g°$, or the volume of carrier gas required to elute a probe from a column containing one gram of the sample of material. $V_g°$ is related to the experimental variables by the following equation:

$$V_g° = (273.15/T_c) \cdot [(t_r - t_m)/W] \cdot F \cdot J \cdot C$$

where C is the correction factor for vapor pressure of water in the soap bubble flowmeter and J is the correction factor for the pressure drop across the column.

$$C = 1 - (P_w/P_0) \qquad (8.10)$$

and

$$J = 1.5 \ [(P_i/P_0)^2 - 1]/[(P_i/P_0)^3 - 1] \tag{8.11}$$

T_c is the column temperature in K; W is the amount of material packed into the column in g; t_r is the retention time of the probe in minutes; t_m is the retention time of a reference probe, such as methane or argon, in minutes; F is the carrier gas flow rate in mL/min.; P_w is the vapor pressure of water at the column temperature in mm Hg; P_0 is the carrier gas pressure at the column outlet (atmospheric pressure) in mm Hg; and P_i is the carrier gas pressure at the column inlet in mm Hg.

8.4.3 TOTAL SURFACE ENERGY

The total surface energy may be regarded as the sum of the contribution of two components: a non-polar and a polar component. The non-polar component is associated with London dispersive forces of interaction, and the polar component is associated with acid-base interactions.

8.4.3.1 Dispersive Component of the Total Surface Energy

The interaction of neutral probes, such as saturated n-alkanes, with the surface of the sample of the material is predominated by London dispersive forces of interaction. Under conditions of infinite dilution of the injected probe vapors, it has been shown that the dispersive component, γ_s^D, of the total surface energy of the material is related to V_g° by the following equation:

$$RT \cdot \ln V_g^\circ \ = \ 2N \left(\gamma_s^D\right)^{1/2} a \left(\gamma_L^D\right)^{1/2} \ + \ C^t \tag{8.12}$$

where N is Avogadro's number, a is the surface area of the probe molecule, γ_L^D is the dispersive component of the surface energy of the probe, and C^t is a constant that depends on the reference states.

A plot of $RT \cdot \ln V_g^\circ$ versus $2N \cdot a(\gamma_L^D)^{1/2}$ should give a straight line with slope, $(\gamma_s^D)^{1/2}$.

8.4.3.2 Acid-Base Component of the Total Surface Energy

The interaction of polar probes with the surface of the material involves both dispersive and acid-base interactions. The free energy of desorption, ΔG_{AB}°, corresponding to specific acid-base interactions can be related to V_g° by the following equation:

$$RT \cdot \ln \left(V_g^\circ / \ V_g^{\circ *}\right) \ = \ \Delta G_{AB}^\circ \tag{8.13}$$

where V_g° is the specific retention volume of the polar probe and $V_g^{\circ *}$ is the specific retention volume of a reference neutral n-alkan.

This equation suggests that values of $RT \cdot \ln V_g^\circ$, plotted against $2N \cdot a(\gamma_L^D)^{1/2}$ for polar probes, should fall above the straight line obtained by plotting $RT \cdot \ln V_g^{\circ *}$ versus $2N \cdot a(\gamma_L^D)^{1/2}$ for the reference neutral n-alkane probes. The difference of ordinates between the point corresponding to the specific polar probe and the reference line gives the value of the free energy of desorption corresponding to the specific acid-base.

The free energy of desorption corresponding to the specific acid-base interactions may be related to the enthalpy of desorption, ΔH_{AB}°, by the following equation:

$$\Delta G_{AB}^\circ = \Delta H_{AB}^\circ - T \Delta S_{AB}^\circ \tag{8.14}$$

TABLE 8.3

Values of the Dispersive Component of the Surface Energy of Lignocellulosics Obtained under Infinite Dilution Conditions

Material	Treatment	γ^D_S at (T °C), mJ/m²	Reference
Cellulose	untreated	48.5 (25°C)	Belgacem (2000)
Wood birch	none	43.8 (50°C)	Kamdem et al. (1993)
Bleached softwood kraft pulp	untreated	37.9 (40°C)	Belgacem (2000)
Lignin	kraft	46.6 (50°C)	Belgacem (2000)
Wood eastern white pine	unextracted	37 (40°C)	Tshabalala (1997)
Kenaf powder	unextracted	40 (40°C)	Tshabalala (1997)
Wood eastern white pine	Extracted with toluene/ethanol (2:1 v/v)	49 (40°C)	Tshabalala (1997)
Kenaf powder	Extracted with toluene/ethanol (2:1 v/v)	42 (40°C)	Tshabalala 1997

where T is the temperature in K and $\Delta S°_{AB}$ is the entropy of desorption corresponding to the specific acid-base interactions. A plot of $\Delta G°_{AB}/T$ versus $1/T$ should yield a straight line with slope $\Delta H°_{AB}$.

It has been shown that the enthalpy of desorption can be used to obtain the acidic and basic constants of a substrate. The acidic and basic constants, K_A and K_B, can be regarded as the acceptor and donor numbers, respectively, and are analogous to the acceptor number, AN*, and donor number, DN, of any compound, as defined by the Gutmann theory of acids and bases. The enthalpy of desorption corresponding to the specific acid-base interactions is related to K_A, K_B, AN*, and DN by the following expression:

$$\Delta H°_{AB} = K_A DN + K_B AN* \tag{8.15}$$

A plot of $\Delta H°_{AB}/AN*$ versus $DN/AN*$ should yield a straight line with slope K_A and intercept K_B. Values of DN and AN* for various solvents are available in the literature (Tshabalala 1997).

IGC has been used to characterize the surfaces of cellulose fibers, birch wood meal, polyethylene and wood pulp fibers, synthetic polymers, and lignocellulosic fibers grafted with poly(methylmethacrylate). The values of the dispersive component of the surface energy of some lignocellulosic materials are summarized in Table 8.3, and Table 8.4 summarizes values of acid-base properties, expressed in terms of the ratio K_A/K_B. For acidic surfaces the value of this ratio is generally greater than 1.0.

TABLE 8.4

Acid-Base Properties of Lignocellulosic Surfaces Obtained under Infinite Dilution Conditions

Material	Treatment	K_A/K_B	Reference
Cellulose powder, 20-μm particle size	none	24	Tshabalala (1997)
Wood birch	none	1.5	Kamdem et al. (1993)
Bleached softwood kraft pulp	untreated	2.2-5.7	Belgacem (2000)
Wood eastern white pine	Extracted with toluene/ethanol (2:1 v/v)	1.4	Tshabalala (1997)
Kenaf powder	unextracted	0	Tshabalala (1997)
Kenaf powder	Extracted with toluene/ethanol (2:1 v/v)	1.6	Tshabalala (1997)

8.5 CONCLUSIONS AND OUTLOOK

Characterization of the surface properties of wood is a very complex and difficult undertaking. No single technique is adequate to completely characterize the surface chemistry of wood and related lignocellulosic materials. Rather, a combination of spectrometric techniques, used together with microscopic and thermodynamic techniques, can provide good insight into the chemical composition of lignocellulosic surfaces, the surface distribution and topography of acid-base sites, and the effect of chemical composition on the reactivity of lignocellulosic surfaces. Hence, as new surface sensitive spectroscopic techniques are applied to the study of lignocellulosic surfaces, it is likely that better data will be developed that should greatly improve our understanding of the surface chemistry of wood. One of the most urgent challenges is the development of a SSIMS spectral database of lignocellulosic materials.

REFERENCES

Adamson, A.W. (1967). *Physical Chemistry of Surfaces* (2nd ed.). Interscience, New York.

Agarwal, U.P. (1999). *An Overview of Raman Spectroscopy as Applied to Lignocellulosic Materials in Advances in Lignocellulosic Characterization* (Dimitris S. Argyropoulos, Ed.). TAPPI Press, Atlanta, GA.

Agarwal, U.P. and Ralph, S.A. (1997). FT-raman spectroscopy of wood: Identifying contributions of lignin and carbohydrate polymers in the spectrum of black spruce (*Picea mariana). Appl. Spectrosc.* 51(11):1648–1655.

Ahmed, A., Adnot, A., and Kaliaguine, S. (1987). ESCA study of solid residues of supercritical extraction of *Populus tremuloides* in methanol. *J. Appl. Polym. Sci.* 34:359–375.

Ahmed, A., Adnot, A., and Kaliaguin, S. (1988). ESCA analysis of partially converted lignocellulosic materials. *J. Appl. Polym. Sci.* 35:1909–1919.

Béland, M.-C. and Mangin, P.J. (1995). *Three-Dimensional Evaluation of Paper Surfaces Using Confocal Microscopy in Surface Analysis of Paper* (Conners, T.E. and Banarjee, S., Eds.). CRC Press, Inc., Boca Raton, FL.

Belgacem, M.N. (2000) Characterisation of polysaccharides, lignin and other woody components by inverse gas chromatography. *Cellulose Chem. Technol.* 34:357–383.

Benninghoven, A., Hagenhoff, B., and Niehuis, E. (1993). Surface MS: Probing real-world samples. *Anal. Chem.* 65(14):630A–640A.

Boyde, A. (1994). Bibliography of Confocal microscopy and its applications. *Scanning* 16:33–56.

Brinen. J.S. (1993). The observation and distribution of organic additives on paper surfaces using surface spectroscopic techniques. *Nordic Pulp Pap. Res. J.* 8:123–129.

Brinen, J.S. and Kulick, R.J. (1995) SIMS imaging of paper surfaces, Part 4: The detection of desizing agents on hard-to-size paper surfaces. *Int. J. Mass Spectrom. Ion Proc.* 143:177–190.

Chtourou, H.B., Reidel, B., and Kokta, B.V. (1995). Surface characterization of modified polyethylene pulp and wood pulp fibers using XPS and inverse gas chromatography. *J. Adhesion Sci. Technol.* 9(5): 551–574.

Comyn, J. (1996). Surface analysis and adhesive bonding. *Anal. Proc.* 30:27–28.

Conley, R.T. (1996). *Infrared Spectroscopy.* Allyn and Bacon, Boston.

Danilatos, G.D. (1988). Foundations of environmental scanning electron microscopy. Advances in Electronics and Electron Physics 71:109–250.

Danilatos, G.D. (1993). Introduction to the ESEM instrument. *Microsc. Res. Tech.* 25:354–361.

Deshmukh, S.C. and Aydil, E.S. (1996). Investigation of low temperature SiO_2 plasma enhanced chemical vapor deposition. *J. Vac. Sci. Technol.* B14:738.

Detter-Hoskin, L.D., and Busc, K.L. (1995). SIMS: Secondary ion mass spectrometry in surface analysis of paper (Conners, T.E. and Banerjee, S.S., Eds.). CRC Press, Inc., Boca Raton, FL.

Donald, A.M. (2003). The use of environmental scanning electron microscopy for imaging wet and insulating materials. *Nat. Mater.* 2(8):511–516.

Donaldson, L. (2003). Private communication. Cell Wall Biotechnology Center, Forest Research, New Zealand.

Dorris, G.M. and Gray, D.G. (1978a). The surface analysis of paper and wood fibres by ESCA I. *Cellulose Chem. Technol.* 12:9–23.

Dorris, G.M. and Gray, D.G. (1978a). The surface analysis of paper and wood fibres by ESCA II. *Cellulose Chem. Technol.* 12:721–734.

Farfard, M., El-Kindi, M., Schreiber, H.P., G. Dipaola-Baranyi, G., and Hor, A.M. (1994.) Estimating surface energy variations of solids by inverse gas chromatography. *J. Adhesion Sci. Technol.* 8(12):1383–1394.

Felix, J.M. and Gatenholm, P. (1993). Characterization of cellulose fibres using inverse gas chromatography. *Nordic Pulp Pap. Res. J.* 1:200–203.

Fowkes, F.M. (1990). Quantitative characterization of the acid-base properties of solvents, polymers and inorganic surfaces. *J. Adhesion Sci. Technol.* 4(8):669–691.

Fracassi, F., d'Agostino, R., and Favia, P. (1992). Plasma – Enhanced chemical vapor-deposition of organosilica thin-films from tetraethoxysilane-oxygen feeds. *J. Electrochem. Soc.* 139(9):2936–2944.

Frisbie, C.D., Rozsnyai, L.F., Noy, A., Wrighton, M.S., and Lieber, C.M. (1994). Functional group imaging by chemical force microscopy. *Science* 265:2071–2074.

Frommer, J. (1992). Scanning tunneling microscopy and atomic force microscopy in organic chemistry. *Angew. Chemie* (int. ed., in English) 31:1298–1328.

Gray, D.G. (1978). The surface analysis of paper and wood fibres by ESCA III. *Cellulose Chem. Technol.* 12:735–743.

Hanley, S.J. and Gray, D.G. (1994). Atomic force microscope images of black spruce wood sections and pulp fines. *Holzforschung* 48(1):29–34.

Hanley, S.J. and Gray, D.G. (1995). Atomic Force Microscopy in Surface Analysis of Paper (Conner, T.E. and Banerjee, S.S., Eds.). CRC Press, Inc. Boca Raton, FL.

Hansma, P.K., Ellings, V.B., Marti, O., and Bracker, C.E. (1998). Scanning tunneling microscopy and atomic force microscopy: Application and technology. *Science* 242:209–216.

Hoh, J.H. and Engel, A. (1993). Friction effects on force measurements with an atomic force microscope. *Langmuir* 9:3310–3312.

Hon, D.N.-S. (1984). ESCA study of oxidized wood surfaces. *J. Appl. Polym. Sci.* 29:2777–2784.

Hon, D.N.-S. and Feist, W.C. (1986). Weathering characteristics of hardwood surfaces. *Wood Sci. Technol.* 20:169–183.

Hua, X., Ben,Y., Kokta, B.V., and Kalinguin, S. (1991). Application of ESCA in wood and pulping chemistry. *China Pulp Pap.* 10:52–57.

Hua, X., Kaliaguine, S., Kokta, B.V., and Adnot, A. (1993a). Surface analysis of explosion pulps by ESAC, Part 1: Carbon (1s) spectra and oxygen-to-carbon ratios. *Wood Sci. Technol.* 27:449–459.

Hua, X., Kaliaguine, S., Kokta, B.V., and Adnot, A, (1993b). Surface analysis of explosion pulps by ESAC, Part 2: Oxygen (1s) and sulfur (2p) spectras. *Wood Sci. Technol.* 28:1–8.

Johnson, D. and Hibbert, S. (1992). Applications of secondary ion mass spectrometry (SIMS) for the analysis of electronic materials. *Semicond. Sci. Technol.* 7:A180–A184.

Kamdem, D.P., Bose, S.K. and Luner, P. (1993). Inverse gas chromatography of birch wood meal. *Langmuir* 9:3039–3044.

Kamdem, D.P. and Reidl, B. (1991). IGC characterization of PMMA grafted onto CTMP fiber. *J. Wood Chem. Technol.* 11(1):57–91.

Kamdem, D.P., Reidl, B., Adnot, A., and Kaliaguine, S. (1991). ESCA spectroscopy of poly(methylmethacrylate) grafted onto wood fibers. *J. Appl. Polym. Sci.* 43:1901–1912.

Lavielle, L. and Schultz, J. (1991). Surface properties of carbon fibers determined by inverse gas chromatography. *Langmuir* 7(5):978–981.

Lee, B.H., Kim, H., Lee, J.J., and Park, M.J. (2003). Effects of acid rain on coatings for exterior wooden panels. *J. Ind. Eng. Chem.* 9(5):500–507.

Leica TCS Confocal Systems User Manual, Version 1.0, January, Leica Microsystems Heidelberg GmbH. Edited and written by EDV-Service Dr. Kehrel, Heidelberg, Germany, 1999.

Li, J-X. and Gardella, J.A., Jr. (1994). Quantitative static secondary ion mass spectrometry of pH effects on octadecylamine monolayer Langmuir-Blodgett films. *Anal. Chem.* 66(7):1032–1037.

Libermann, M.A. and Lichtenberg, A.J. (1994). *Principles of Plasma Discharges and Materials Processing.* John Wiley & Sons, New York.

Lichtman, J.W. (1994) Confocal microscopy. *Sci. Am.* 271:40–45.

Louder, D.R. and Parkinson, B.A. (1995). An update on scanning force microscopies. *Anal. Chem.* 67(9):297A–303A.

Loxton, C., Thumm, A., Grisby, W.J., Adams, T.A., and Ede, R.M. (2003). Resin distribution in medium density fiberboard: Quantification of UF resin distribution on blowline- and dry-blended MDF fiber and panels. *Wood Fiber Sci.* 35(3):370–380.

McGhie, A.J., Tang, S.L., and Li, S.F.Y. (1995). Expanding the uses of AFM. *Chemtech* 25(7):20–26.

Meredith, P., Donald, A.M., and Thiel, B. (1996). Electron-gas interactions in the environmental SEM's gaseous detector. *Scanning* 18:467–473.

Meyer, E. (1992). Atomic force microscopy. *Prog. in Surf. Sci.* 41:3–49.

Mirabella, F.M. (Ed.) (1998). *Modern Techniques in Applied Molecular Spectroscopy.* John Wiley & Sons, New York.

Mjörberg, P.J. (1981). Chemical surface analysis of wood fibres by means of ESCA. *Cellulose Chem. Technol.* 15:481–486.

Nguyen, T. and John, W.E. (1978). Polar and dispersion force contributions to the total surface free energy of wood. *Wood Sci. Technol.* 12:63–74.

Pachuta, S.J. and Staral, J.S. (1994). Nondestructive analysis of colorants on paper by time-of-flight secondary ion mass spectrometry. *Anal. Chem.* 66(2):276–284.

Pandey, K.K. and Theagarajan, K.S. (1997). Analysis of wood surfaces and ground wood by diffuse reflectance (DRIFT) and photoacoustic (PAS) Fourier transform spectroscopic techniques. *Holz als Roh- und Werkstoff* 55:383–390.

Pawley, J.B. (1990) *The Handbook of Biological Confocal Microscopy.* Plenum Press, New York.

Perry, S.S. and Somorjai, G.A. (1994). Characterization of organic surfaces. *Anal. Chem.* 66(7):403A–415A.

Rynders, R.M., Hegedus, C.R., and Gilicinski, A.G. (1995). Characterization of particle coalescence in waterborne coatings using atomic force microscopy. *J. Coat. Technol.* 667(845):59–69.

Sahli, S., Segui, Y., Ramdani, R., and Takkouk, Z. (1994). RF plasma deposition from hexamethyldisiloxane oxygen mixtures. *Thin Solid Films* 250(1–2):206–212.

Schaefer, D.M., Carpenter, M., Gady, B., Reifenberger, R., Demejo, L.P., and Rimai, D.S. (1995). Surface roughness and its influence on particle adhesion using atomic force techniques. *J. Adhesion Sci. Technol.* 9(8):1049–1062.

Selamoglu, N., Mucha, J.A., Ibbotson, D.E., and Flamm, D.L. (1989). Silicon oxide deposition from tetraethoxy-silane in Radio-Frequency down stream reactor mechanisms and stop coverage. *J. Vac. Sci. Technol.* B7:1345.

Schultz, J. and Lavielle, L. (1989). Interfacial properties of carbon fiber-epoxy matrix composites. In: Lloyd, D.R., Ward, T.C., and Schreiber, H.P. (Eds.), *Inverse Gas Chromatography* [ACS symposium series] 391:168–184.

Stuart, B.H. (2004). *Infrared Spectroscopy – Fundamentals and Applications.* John Wiley & Sons, New York.

Tan, Z. and Reeve, D.W. (1992). Spatial distribution of organochlorine in fully bleached kraft pulp fibres. *Nordic Pulp Pap. Res. J.* 6:30–36.

Tshabalala, M.A. (1997). Determination of acid-base characteristics of lignocellulosic surfaces by inverse gas chromatography. *J. Appl. Polym. Sci.* 65:1013–1020.

Tshabalala, M.A., Kingshott, P., VanLandingham, M.R., and Plackett, D. (2003). Surface chemistry and moisture sorption properties of wood coated with multifunctional alkoxysilanes by sol-gel process. *J. Appl. Polym. Sci.* 88(12):2828–2841.

Watts, J.F. (1990). *An Introduction to Surface Analysis by Electron Spectroscopy.* Oxford University Press, New York.

Watts, J.F. (1992). Investigation of adhesion phenomena using surface analytical techniques. *Anal. Proc.* 29:396–398.

Williams, D. (1994). Inverse gas chromatography. In: Ishida, H. (Ed.), *Characterization of Composite Materials.* Butterworth-Heinemann, Boston, MA.

Williams, R.S. and Feist, W.C. (1984). Application of ESCA to evaluate wood and cellulose surfaces modified by aqueous chromium trioxide treatment. *Colloids Surf.* 9:253–271.

Winograd, N. (1993). Ion beams and laser positionization for molecule-specific imaging. *Anal. Chem.* 65(14):622A–629A.

Young, R.A., Rammon, R.M., Kelley, S.S., and Gillespie, R.H. (1982). Bond formation by wood surface reactions, Part I: Surface analysis by ESCA. *Wood Sci.* 14:100–119.